Available online at www.sciencedirect.com
ScienceDirect
Journal of Sound and Vibration 321 (2009) 680–703
JOURNAL OF SOUND AND VIBRATION
www.elsevier.com/locate/jsvi

Turbulence effects on fluidelastic instability of a cylinder in a shear flow

Jinyu Zhu[a], X.Q. Wang[b,*], Wei-Chau Xie[a], R.M.C. So[b]

[a]Department of Civil and Environmental Engineering, Faculty of Engineering, University of Waterloo, Waterloo, Ontario, Canada N2L 3G1
[b]Department of Mechanical Engineering, The Hong Kong Polytechnic University, Hung Hom, Kowloon, Hong Kong

Received 2 October 2007; received in revised form 19 September 2008; accepted 24 September 2008
Handling Editor: L.G. Tham
Available online 18 November 2008

Abstract

Fluidelastic instability is the main mechanism that causes severe damages in flow-induced vibration. Experiments show that grid-generated turbulence can affect the stability of the system, which is modeled as an Ornstein–Uhlenbeck process. The dynamic stability of a four-dimensional system under real noise excitation is studied through the determination of the p th moment Lyapunov exponent and the Lyapunov exponent. The partial differential eigenvalue equation governing the moment Lyapunov exponent is established. For small noise amplitudes, a method of regular perturbation is used to determine analytical expansions of the moment Lyapunov exponents and Lyapunov exponents, which are shown to be in good agreement with those obtained using numerical approaches. The analytical method is applied to study the stability of a cylinder in a shear flow, where fluidelastic instability is known to occur. The results demonstrate that the unstable system can be stabilized under certain conditions and the effect of stabilization is proportional to the turbulence intensity, which agrees with experimental observations.

1. Introduction

Three mechanisms are usually considered to be responsible for flow-induced vibration and/or instability of a cylinder in a cross-flow; they are vortex-induced lock-in resonance, fluidelastic instability, and turbulence-induced buffeting. According to Naudascher and Rockwell [1], these three mechanisms represent three general sources of excitation: the (flow) instability-induced excitation (IIE), the movement-induced excitation (MIE), and the extraneously excited excitation (EIE), respectively. The total flow-induced force can then be expressed as

$$F = F_V + F_M + F_T, \tag{1}$$

where the subscripts V, M, and T represent vortex-induced, motion-dependent, and turbulence-induced buffeting forces, respectively. When the cylinder is rigid and fixed, its behavior becomes stationary even though there is a

*Corresponding author. Department of Mechanical and Aerospace Engineering, Arizona State University, Tempe, AZ 85287, USA. Tel.: +1 480 965 4294.
E-mail addresses: julianxqwang@hotmail.com, julianxqwang@gmail.com (X.Q. Wang).

0022-460X/$ - see front matter © 2008 Elsevier Ltd. All rights reserved.
doi:10.1016/j.jsv.2008.09.048

cross-flow. In this case, the total flow-induced force becomes

$$F_0 = F_{V0} + F_{T0}. \tag{2}$$

The three mechanisms may co-exist in any flow-induced vibration problem. When that happens, the dynamic behavior of the fluid–structure system becomes very complex. The tasks of a theoretical modeling study are to formulate the problem in a general way, to simplify the formulation by identifying key mechanism(s), and to demonstrate the main features for specific cases through dynamic analyses. In the present study, a single circular cylinder in a shear flow with free-stream turbulence is considered. The aim of the investigation is to identify the mechanisms that contribute to fluid–structure instability and to analyze the effect of free-stream turbulence in detail.

For a single circular cylinder in a uniform flow, the main mechanism of unstable motion is considered to be vortex-induced lock-in resonance [2,3]. In a recent modeling study, Zhu et al. [4] showed that this lock-in resonance is accompanied by a parametric instability due to the fluid-damping force. On the other hand, Yu et al. [5] showed that a single cylinder can undergo fluidelastic instability if the approach flow is not uniform, e.g., a shear flow. Such instability occurs at very large values of reduced velocity ($U_r > 100$), where the vortex-induced force has no appreciable influence on cylinder vibration. The main mechanism responsible for this type of instability can be attributed to changes in the mean lift and mean drag force relative to cylinder motion. Fluidelastic instability may also occur when the single cylinder is in the wake of another cylinder [6], or in cylinder arrays [7,8]. The motion-dependent fluid force, in the form of fluid-damping force and/or fluid-stiffness force, is responsible for fluidelastic instability in these cases.

Since fluidelastic instability can occur under different circumstances, its suppression is thus of importance to a variety of engineering applications. In practical engineering problems, the flow is most likely turbulent. According to So and Savkar [9], under certain flow conditions, free-stream turbulence can act to substantially increase the fluctuating vortex-induced forces on a rigid cylinder. Their measurements were carried out on rigid cylinders. The increased fluctuating forces can, in turn, influence the fluidelastic instability of the fluid–structure system. Romberg and Popp [10] presented some interesting stability results from experiments carried out on flow-induced vibrations of a flexibly mounted cylinder within an array of fixed cylinders. They considered both fluidelastic instability and turbulent buffeting, and showed that large galloping motion can be stabilized by grid-generated turbulence. In one of their experiments, Romberg and Popp [10] considered a cylinder with very small structural damping. The total damping measured in the flow direction is high, and the cylinder undergoes a galloping motion in the cross-flow (lift) direction at a certain reduced velocity $U_{r,\mathrm{cr}}$. Turbulence occurs in cylinder bundles due to upstream cylinder bundles acting as turbulence generators. Additional turbulence was generated in this experiment by placing a turbulence grid at a specified distance in front of the flexibly mounted cylinder. It was observed that as the upstream turbulence was increased in the flow, a significant stabilization took place and the galloping instability did not occur for reduced velocity values substantially higher than $U_{r,\mathrm{cr}}$. The experiment also showed that turbulence intensity is a significant factor influencing stability. Similar effects were observed in the experiments of a parallel triangular tube bundle performed by Rottmann and Popp [11].

The stabilizing effect of turbulence has also been reported in the literature for bridge structures under turbulent winds (e.g. Ref. [12]). An intuitive explanation has been given which states that turbulence may help to transfer energy from the least stable mode to the more stable modes. Therefore, coupled modes have to be considered in the stability analysis. In the study of stochastic dynamical systems, stabilizing a system by noise is an important topic (e.g. Refs. [13,14]). For linear systems it is found that stabilization by white noise is possible if and only if the trace of the system matrix, i.e. the sum of the eigenvalues, is negative. Pandey and Ariaratnam [15] analyzed the stability of wind-induced torsional motion of slender bridges under stochastic wind turbulence. They used a periodic excitation with random phase modulation to model turbulence in the wind velocity. They found that turbulence has a small stabilizing effect on the bridge stability, although an increase in the bandwidth of the excitation process does tend to stabilize the bridge motion. Rzentkowski and Lever [16] used a nonlinear model to study turbulence effect on fluidelastic instability in tube arrays and found that turbulence either reduces or has negligible effect on the stability boundary depending on the vibration pattern.

Poirel and Price [17] also found that turbulence could lower the speed of flutter of a two-dimensional airfoil. They used the Dryden model to represent longitudinal turbulence. The stability boundary was determined by obtaining the largest Lyapunov exponent via Monte Carlo simulation. Namachchivaya and Vedula [18] theoretically proved that a four-dimensional system could be stabilized by real noise. They used a second-order filter to model the noise and examined the moment stability and sample stability of the system by obtaining the moment Lyapunov exponent and Lyapunov exponent. However, they did not validate the analytical results by comparing with numerical results obtained by Monte Carlo simulation. The noise is very narrow-banded, which seems to be unrealistic for practical turbulence. For more information, Ibrahim [19] gave a detailed review about the noise effects, including stabilization by multiplicative noise and noise-enhanced stability (NES), noise-induced transition, and stochastic resonance, on the stability of dynamical systems.

In the present study, the model developed in the previous study [4] is extended to take the effects of shear flow and free-stream turbulence into account. A general nonlinear model is first proposed, then reduced to a linear one for dynamic analysis of a single spring-supported cylinder in a turbulent shear flow at large U_r values. Thus, the fluidelastic instability of the cylinder is studied, and the suppression of such instability by free-stream turbulence in the approach flow is demonstrated through a stability analysis. The stochastic stability of structures is introduced in Section 2.

Since grid-generated turbulence is nearly stationary and Gaussian, the fluctuating velocity in this type of turbulent flow is modeled as an Ornstein–Uhlenbeck process. An analytical model developed by Zhu et al. [4] is extended to represent the vortex-induced force on the cylinder in the case of shear flow. Finally, the randomized equations of motion are obtained by substituting the expressions for the random velocity into the original deterministic equations of motion, as is described in Section 3.

In Section 4, the dynamic stability of a four-dimensional system under real noise excitation is studied through the determination of the p th moment Lyapunov exponent and the Lyapunov exponent. The partial differential eigenvalue equation governing the moment Lyapunov exponent is established. For small noise amplitudes, a method of regular perturbation is applied to determine analytical expansions of the moment Lyapunov exponents and Lyapunov exponents. In this way, both the sample stability and moment stability are studied.

In Section 5, the stability of the deterministic system is studied by varying the critical parameter (natural frequency ratio k). The analytical results obtained in Section 4 are used to explore the stochastic stability of a cylinder in a shear flow. It is shown that fluidelastic instability can be stabilized by turbulence under certain conditions. Parametric studies are performed to demonstrate the significant effects of noise parameters α and σ on the stability of the cylinder. Analytical results and numerical simulations are compared to validate the approach.

2. Dynamic stability of structures

The equation of motion for many flow-induced vibration problems is of the general form

$$q''(\tau) + [2\varepsilon_0\beta + \varepsilon_0\mu\zeta(\tau)]q'(\tau) + \omega_0^2 q(\tau) + f[q, q', \varepsilon_0\zeta(\tau)] = 0, \tag{3}$$

where the prime denotes differentiation with respect to the time variable τ, q is the generalized coordinate, β is the damping constant, ω_0 is the circular natural frequency, ε_0 is a small fluctuation parameter, $f[q, q', \varepsilon_0\zeta(\tau)]$ is a nonlinear function, and $\zeta(\tau)$ is a stochastic process that describes the random nature of the flow.

It is natural to ask how the parametric random fluctuation $\zeta(\tau)$ can influence the dynamic stability of system (3). The dynamical stability of the trivial solution of system (3) is governed by the stability of the trivial solution of the linearized equation

$$q''(\tau) + [2\varepsilon_0\beta + \varepsilon_0\mu\zeta(\tau)]q'(\tau) + \omega_0^2 q(\tau) = 0. \tag{4}$$

The sample or almost-sure stability of the trivial solution of system (4) is determined by the Lyapunov exponent, which characterizes the average exponential rate of growth of the solutions of system (4) for large τ

and is defined as

$$\lambda_{q(\tau)} = \lim_{\tau\to\infty} \frac{1}{\tau} \log \|\mathbf{q}(\tau)\|, \tag{5}$$

where $\mathbf{q}(\tau) = \{q(\tau), q'(\tau)\}^{\mathrm{T}}$ and $\|\mathbf{q}\| = (\mathbf{q}^{\mathrm{T}}\mathbf{q})^{1/2}$ is the Euclidean norm. If the largest Lyapunov exponent is negative, the trivial solution of system (4) is stable with probability 1; otherwise, it is almost surely unstable.

On the other hand, the stability of the p th moment $\mathsf{E}[\|\mathbf{q}\|^p]$ of the solution of system (4) is governed by the p th moment Lyapunov exponent defined by

$$\Lambda_{q(\tau)}(p) = \lim_{\tau\to\infty} \frac{1}{\tau} \log \mathsf{E}[\|\mathbf{q}\|^p], \tag{6}$$

where $\mathsf{E}[\cdot]$ denotes the expected value. If $\Lambda_{q(\tau)}(p)$ is negative, then the p th moment is stable; otherwise, it is unstable. The relationship between the sample stability and the moment stability was formulated by Arnold [20]. The p th moment Lyapunov exponent $\Lambda_{q(\tau)}(p)$ is a convex analytic function in p that passes through the origin and the slope at the origin is equal to the largest Lyapunov exponent $\lambda_{q(\tau)}$, i.e.

$$\lambda_{q(\tau)} = \lim_{p\to 0} \frac{\Lambda_{q(\tau)}(p)}{p}. \tag{7}$$

The moment Lyapunov exponents are important in obtaining a complete picture of the dynamic stability of the trivial solution of system (4). Suppose the largest Lyapunov exponent $\lambda_{q(\tau)}$ is negative, implying that the trivial solution of system (4) is sample stable. However, the p th moment typically grows exponentially for large enough p, implying that the p th moment of the trivial solution is unstable. The latter can be explained by large deviation. While there is the solution of the system $\|\mathbf{q}\| \to 0$ as $\tau \to \infty$ with probability one at an exponential rate $\lambda_{q(\tau)}$, there is also small probability that $\|\mathbf{q}\|$ is large, which makes the expected value $\mathsf{E}[\|\mathbf{q}\|^p]$ of this rare event large for large enough values of p. This leads to the p th moment instability.

A systematic study of moment Lyapunov exponents is presented by Arnold et al. [21] for linear Itô systems and by Arnold et al. [22] for linear stochastic systems under real noise excitations. The theory and techniques of studying the stability of stochastic systems can be found in Xie [23].

3. Modeling of a spring-supported cylinder in shear flow

3.1. Deterministic modeling

Consider an elastically supported rigid cylinder in a cross-flow. The approach flow is assumed to be a linear shear flow and two-dimensional. The equations of motion of the cylinder can be written as

$$\ddot{x}(t) + 2\zeta_s\omega_x\dot{x}(t) + \omega_x^2 x(t) = \frac{F^X(t)}{M}, \tag{8a}$$

$$\ddot{y}(t) + 2\zeta_s\omega_y\dot{y}(t) + \omega_y^2 y(t) = \frac{F^Y(t)}{M}, \tag{8b}$$

where $x(t)$ and $y(t)$ are cylinder displacements in the stream-wise and the cross-flow directions, respectively, $\omega_{x/y}$ is the natural frequency, ζ_s is the structural damping coefficient, and M is the mass per unit length of the cylinder. In Eqs. (8a), (8b), $F^X(t)$ and $F^Y(t)$ are flow-induced forces per unit length acting on the cylinder in the stream-wise and the cross-flow directions, respectively. For the present case, flow-induced forces may be divided into two components: one arising from vortex shedding, and the other due to the feedback effect of cylinder motion. Hence, they can be written as

$$F^X(t) = F_V^X(t) + F_M^X(t),$$

$$F^Y(t) = F_V^Y(t) + F_M^Y(t),$$

where the subscripts "V" and "M" represent "vortex-induced" and "motion-dependent", respectively.

When the cylinder is stationary, the motion-dependent fluid forces, $F_M^X(t)$ and $F_M^Y(t)$, are absent, and only vortex-induced forces are applied to the cylinder. These are denoted as $F_{V_0}^X(t)$ and $F_{V_0}^Y(t)$ in order to differentiate them from their counterparts when the cylinder is in motion. Once the cylinder is vibrating under the action of vortex-induced forces, its motion can alter the vortex shedding behavior, thus changing vortex-induced forces not only in their magnitudes but also in their dominant frequencies. In addition to vortex-induced excitation, fluid flow will also affect the dynamics of the cylinder in the form of added mass, fluid damping, etc. They are all included in the motion-dependent forces, $F_M^X(t)$ and $F_M^Y(t)$, in the present formulation.

In general, both vortex-induced and motion-dependent forces are unsteady, and their amplitudes are nonlinearly dependent on a number of parameters, such as the Reynolds number, the reduced velocity, structural damping, etc. Their exact expressions are thus complex and difficult to determine. In order for a theoretical analysis to be carried out, approximate modeling is necessary.

3.2. Modeling of motion-dependent forces

Cylinder vibration induces fluid forces, such as the added mass and the fluid damping force. In the present study, they are approximated as the linear combination

$$\begin{bmatrix} F_M^X \\ F_M^Y \end{bmatrix} = -\frac{\rho\pi D^2}{4}\begin{bmatrix} c_m^x & c_m^{xy} \\ c_m^{yx} & c_m^y \end{bmatrix}\begin{bmatrix} \ddot{x} \\ \ddot{y} \end{bmatrix} + \frac{\rho U^2}{\omega_0}\begin{bmatrix} c_d^x & c_d^{xy} \\ c_d^{yx} & c_d^y \end{bmatrix}\begin{bmatrix} \dot{x} \\ \dot{y} \end{bmatrix} + \rho U^2\begin{bmatrix} c_k^x & c_k^{xy} \\ c_k^{yx} & c_k^y \end{bmatrix}\begin{bmatrix} x \\ y \end{bmatrix}, \tag{9}$$

where c_m, c_d, and c_k are the added mass, the fluid damping, and the fluid-stiffness coefficients, respectively. In general, the added mass is considered to be equal to the mass of fluid displaced by the vibrating cylinder. As a first approximation, the fluid damping force is assumed to be proportional to the velocity of cylinder vibration. The fluid-stiffness term only affects the natural frequency of the fluid–structure system.

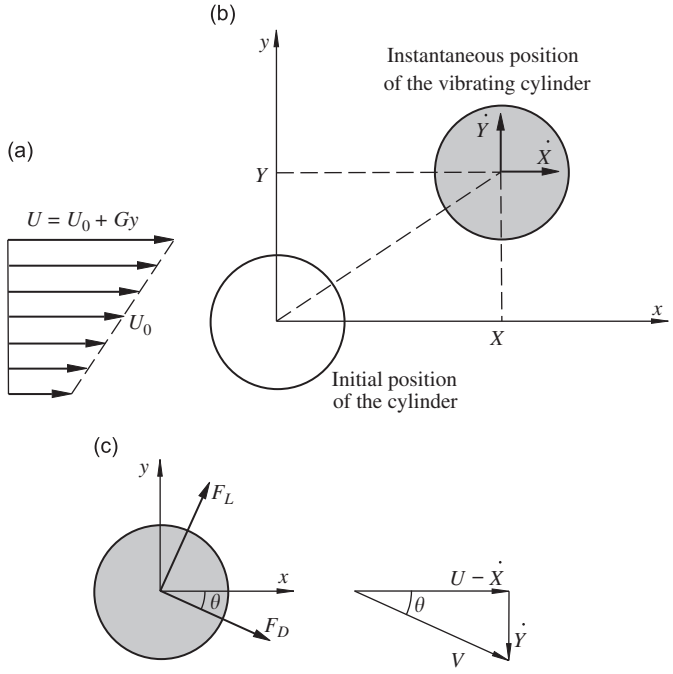

Fig. 1. Illustration of the flow-induced forces. (a) A cylinder subjected to a shear flow; (b) drag and lift forces acting on the vibrating cylinder.

3.3. Modeling of vortex-induced forces

The model developed by Zhu et al. [4] is extended to represent vortex-induced forces acting on a vibrating cylinder in shear flow. The basic idea of this model is illustrated in Fig. 1. According to the model, when the velocity of cylinder vibration is small compared with the flow velocity, it is assumed that the unsteady vortex-induced forces acting on the vibrating cylinder are equal to the vortex-induced forces acting on a similar stationary cylinder, but with the direction of the approach flow changed by the velocity of cylinder vibration. For a stationary cylinder, the vortex-induced forces are also stationary and can be represented by the bounded noise processes. Vortex-induced forces can be thus expressed as

$$F_V^X(t) = C_{V_0}^X(t) \cdot \cos\theta(t) + C_{V_0}^Y(t) \cdot \sin\theta(t), \tag{10a}$$

$$F_V^Y(t) = C_{V_0}^Y(t) \cdot \cos\theta(t) - C_{V_0}^X(t) \cdot \sin\theta(t), \tag{10b}$$

where $C_{V_0}^X(t)$ and $C_{V_0}^Y(t)$ are the drag and lift forces acting on the stationary cylinder, θ is the angle between the x-axis and the instantaneous velocity vector of cylinder vibration given by

$$\theta(t) = \tan^{-1}\frac{\dot{y}}{U - \dot{x}}.$$

In a shear flow, the force coefficients can be expanded in terms of displacements (assumed to be small) of the cylinder about its original position (0, 0), i.e.,

$$C_{V_0}^X(t) = \frac{1}{2}\rho V^2 D\left[C_D(0,0,t) + \frac{\partial C_D(0,0,t)}{\partial x}x + \frac{\partial C_D(0,0,t)}{\partial y}y\right],$$

$$C_{V_0}^Y(t) = \frac{1}{2}\rho V^2 D\left[C_L(0,0,t) + \frac{\partial C_L(0,0,t)}{\partial x}x + \frac{\partial C_L(0,0,t)}{\partial y}y\right],$$

where V is the relative velocity. The local velocity is also a function of the coordinate y only, i.e., $U = U_0 + Gy$, where G is the shear gradient; therefore, the derivatives with respect to x are zero in the above expressions, i.e., $\partial C_D/\partial x = \partial C_L/\partial x = 0$. When the cylinder velocity is much smaller than the flow velocity, i.e., $\dot{x}(t) \ll U$ and $\dot{y}(t) \ll U$, the relative velocity can be approximated as

$$V^2(t) = (U_0 + Gy - \dot{x})^2 + \dot{y}^2 \approx U_0^2\left(1 + 2\frac{Gy - \dot{x}}{U_0}\right).$$

Indeed, Eqs. (8)–(10) represent a nonlinear force evolution process. From Eqs. (8a), (8b), it can be seen that vortex-induced forces excite the cylinder as a component of flow-induced forces and, in turn, the cylinder response modifies vortex-induced forces according to Eqs. (10a), (10b). This interaction keeps evolving until a dynamic steady state is reached. In general, the final vortex-induced forces are nonlinear [24]. If the approach flow has a constant shear and turbulent, as considered in the present study, the resulting equations of motion become very complicated. As a first attempt, a linear approximation is made in the present study for small amplitude vibration, i.e.,

$$\sin\theta(t) = \frac{\dot{y}(t)}{\sqrt{[U_0 + Gy - \dot{x}(t)]^2 + \dot{y}^2(t)}} \approx \frac{\dot{y}(t)}{U_0},$$

$$\cos\theta(t) = \frac{U_0 + Gy - \dot{x}(t)}{\sqrt{[U_0 + Gy - \dot{x}(t)]^2 + \dot{y}^2(t)}} \approx 1.$$

Substituting the above approximate expressions into Eqs. (10a), (10b), the vortex forces can be written as

$$F_V^X = \frac{1}{2}\rho U_0^2 D\left(C_D + \frac{\partial C_D}{\partial y}y + 2\frac{Gy-\dot{x}}{U_0}C_D + \frac{\dot{y}}{U_0}C_L\right), \tag{11a}$$

$$F_V^Y = \frac{1}{2}\rho U_0^2 D\left(C_L + \frac{\partial C_L}{\partial y}y + 2\frac{Gy-\dot{x}}{U_0}C_L - \frac{\dot{y}}{U_0}C_D\right). \tag{11b}$$

3.4. Modeling of grid-generated turbulence

Free-stream turbulence is considered as a disturbance to the approach flow velocity. This disturbance, in turn, affects the fluid forces applied to the cylinder. Due to the random nature of turbulence, statistical methods are commonly used to describe its behavior. Grid-generated turbulence is approximately stationary, homogeneous, and isotropic (see, e.g., Ref. [25]), and can therefore be modeled by a stochastic process. To simplify the problem, only the turbulence in the stream direction is considered.

For the case of one-dimensional flow, the flow velocity can be written as the sum of the mean value $\bar{U}$ and the fluctuating part $\tilde{U}$

$$U(t) = \bar{U} + \tilde{U} = \bar{U} + \eta(t),$$

where $\eta(t)$ is a random process of mean zero. Experiments (see, e.g., Ref. [25]) have shown that the space correlation function $f(r)$ has the form

$$f(r) = f(0)\exp[-r/L_x],$$

where r is the distance between two correlated points in the x-direction, and L_x is the integral length scale. If the field of fluctuating velocity is superimposed on a mean flow of velocity $\bar{U}$ in the x-direction, and if the turbulence is small compared with the mean flow, the turbulence can be thought of being convected by the mean velocity $\bar{U}$ without evolution, which is known as Taylor's hypothesis. Thus, it is possible to interchange time and space variables. The correlation function in time is related to the correlation function in space by replacing the time τ by $r/\bar{U}$, i.e.

$$\langle\tilde{U}(t)\tilde{U}(t+\tau)\rangle = R(\tau) = f(\tau U), \tag{12}$$

where $R(\tau)$ is the correlation function in time. Hence, the corresponding time correlation function is given by

$$R(\tau) = f(\tau U) = R(0)\exp[-|\tau|\bar{U}/L_x]. \tag{13}$$

Since $R(0) = f(0) = \sigma_x^2 = \langle\tilde{U}^2(t)\rangle$ (σ_x is the root-mean-square of the turbulent velocity fluctuations), the time correlation function (13) at some fixed point in the flow field can be described by

$$R(\tau) = \sigma_x^2\exp[-|\tau|\bar{U}/L_x]. \tag{14}$$

Based on experimental observations of grid-generated turbulence, the fluctuating velocity $\tilde{U}$ can be modeled as an Ornstein–Uhlenbeck process (see, e.g., Ref. [26]). An Ornstein–Uhlenbeck process $\eta(t)$ is defined by the one-dimensional Itô stochastic differential equation

$$\mathrm{d}\eta(t) = -\alpha\,\eta(t)\,\mathrm{d}t + \sigma\,\mathrm{d}W(t), \quad \eta(t_0) = \eta_0,$$

where α and σ are constants. The probability density function $f(\eta, t)$ is described by the Fokker–Planck equation

$$\frac{\partial f}{\partial t} = \frac{\sigma^2}{2}\frac{\partial^2 f}{\partial \eta^2} + \alpha\frac{\partial(f\eta)}{\partial\eta}. \tag{15}$$

If the initial condition η_0 is normal with mean 0 and variance $\sigma^2/(2\alpha)$, i.e., $\eta_0 \sim N(0, \sigma^2/(2\alpha))$, then $\eta(t)$ is a stationary Gaussian process with mean zero, $\mathsf{E}[\eta(t)] = 0$, and the correlation function is given by

$$R(\tau) = \mathsf{E}[\eta(t)\,\eta(t+\tau)] = \frac{\sigma^2}{2\alpha}\mathrm{e}^{-\alpha|\tau|}. \tag{16}$$

An Ornstein–Uhlenbeck process is a simple, Gaussian, explicitly representable stationary process that is often used to model a realizable noise process. As a result, it is also referred to as a real noise process. A limitation of an Ornstein–Uhlenbeck process is that $\eta(t)$ is nowhere differentiable, which is unrealistic in most cases. For further details, refer to the book by Pope [26]. Comparing the correlation function of the grid-generated turbulence (Eq. (14)) with that of an Ornstein–Uhlenbeck process (Eq. (16)), one obtains

$$\sigma = \sqrt{\frac{2\bar{U}}{L_x}}\sigma_x, \quad \alpha = \frac{\bar{U}}{L_x}.$$

For the following perturbation analysis, let

$$\eta(t) = \sigma_0 \xi(t),$$

where σ_0 is a small parameter. By following Ito's formula, one can obtain the governing stochastic differential equation for $\xi(t)$, i.e.

$$\mathrm{d}\xi(t) = -\alpha\,\xi(t)\,\mathrm{d}t + \sigma_\xi\,\mathrm{d}W(t), \quad \xi(t_0) = \xi_0,$$

where $\sigma_\xi = \sigma/\sigma_0$.

3.5. Randomizing equations of motion

Since the fluctuating velocity is small compared to the mean velocity $\bar{U} = U_0$, one has the following approximation:

$$U^2 = U_0^2\left(1 + \frac{\sigma_0}{U_0}\xi(t)\right)^2 \approx U_0^2(1 + 2\mu\xi(t)),$$

where $\mu = \sigma_0/U_0$ is the noise intensity. By replacing the deterministic velocity U_0 with the turbulent velocity $U = U_0(1 + \mu\xi(t))$ and substituting the above approximate expression for U^2 into Eqs. (11a), (11b), one obtains

$$F_{VT}^X = \frac{1}{2}\rho U_0^2 D[1 + 2\mu\xi(t)]\left(C_D + \frac{\partial C_D}{\partial y}y\right) + \frac{1}{2}\rho U_0 D[1 + \mu\xi(t)][2(Gy - \dot{x})C_D + \dot{y}C_L], \tag{17a}$$

$$F_{VT}^Y = \frac{1}{2}\rho U_0^2 D[1 + 2\mu\xi(t)]\left(C_L + \frac{\partial C_L}{\partial y}y\right) + \frac{1}{2}\rho U_0 D[1 + \mu\xi(t)][2(Gy - \dot{x})C_L - \dot{y}C_D], \tag{17b}$$

where the subscript "T" means that the turbulence effect on the vortex-induced force is included. Similarly, the randomized motion-dependent force is given by

$$\begin{Bmatrix} F_{MT}^X \\ F_{MT}^Y \end{Bmatrix} = -\frac{\rho\pi D^2}{4}\begin{bmatrix} c_m^x & c_m^{xy} \\ c_m^{yx} & c_m^y \end{bmatrix}\begin{Bmatrix} \ddot{x} \\ \ddot{y} \end{Bmatrix} + \frac{\rho U_0^2[1 + 2\mu\xi(t)]}{\omega_0}\begin{bmatrix} c_d^x & c_d^{xy} \\ c_d^{yx} & c_d^y \end{bmatrix}\begin{Bmatrix} \dot{x} \\ \dot{y} \end{Bmatrix} + \rho U_0^2[1 + 2\mu\xi(t)]\begin{bmatrix} c_k^x & c_k^{xy} \\ c_k^{yx} & c_k^y \end{bmatrix}\begin{Bmatrix} x \\ y \end{Bmatrix}. \tag{18}$$

Substituting Eqs. (17) and (18) into Eq. (8), one can obtain the equations of motion for a cylinder in a turbulent shear flow, which includes the vortex-induced force, the motion-dependent force, and turbulence. When the effects of free-stream turbulence and shear flow are removed, this general model is reduced to the model of Zhu et al. [4] for a cylinder in a uniform cross-flow. Zhu et al. [4] showed that parametric resonance could occur as a result of an interaction between the x- and y-direction motion in the lock-in range. Both the motion-dependent force and vortex shedding play a significant role in the vibration.

Yu et al. [5] found experimentally that fluidelastic instability could occur at high reduced velocity ($U_r > 100$) from $Re = 8$ to 120. At this range of high U_r, the experimental results of Chen et al. [30] showed that the motion-dependent damping and stiffness forces approached zero for a single cylinder in a cross-flow, and can be neglected. Using these findings, the model considered here reduces to that of Yu et al. [5].

Nondimensionalizing the equations of motion with respect to U_0 and D, and applying the time scaling $\tau = \omega_x t$, the equations of motion become

$$X'' + \left[2\zeta + \frac{U_r(1+\mu\xi(\tau))C_D}{M_r}\right]X' + X - \left[\frac{U_r^2(1+2\mu\xi(\tau))}{2M_r}\frac{\partial C_D}{\partial Y} + \frac{U_r^2(1+2\mu\xi(\tau))KC_D}{M_r}\right]Y - \frac{U_r(1+\mu\xi(\tau))C_L}{2M_r}Y' = \frac{U_r^2(1+2\mu\xi(\tau))C_D}{2M_r}, \tag{19a}$$

$$Y'' + k\left[2\zeta + \frac{U_r(1+\mu\xi(\tau))C_D}{2M_r}\right]Y' + k^2\left[1 - \frac{U_r^2(1+2\mu\xi(\tau))}{2M_r}\frac{\partial C_L}{\partial Y} - \frac{U_r^2(1+2\mu\xi(\tau))KC_L}{M_r}\right]Y + \frac{kU_r(1+2\mu\xi(\tau))C_L}{M_r}X' = \frac{k^2U_r^2(1+2\mu\xi(\tau))C_L}{2M_r}, \tag{19b}$$

where

$$M_r = \frac{M}{\rho D^2}, \quad K = \frac{GD}{U_0}, \quad U_r = \frac{U_0}{\omega_x D}, \quad k = \frac{\omega_y}{\omega_x}, \quad X = \frac{x}{D}, \quad Y = \frac{y}{D}.$$

At this range of Reynolds number, the shedding frequency varies slightly between 0.13 and 0.2 [27], which is far removed from the natural frequencies of the cylinder. In addition, the mass ratio of the cylinder considered here is quite large ($M_r = 5112$). Hence, the forced vibration due to vortex shedding is negligible. Furthermore, additive noise does not affect the stability of the system [19]. For the analysis of fluidelastic instability, one can neglect the force terms in the right-hand-side of Eqs. (19a), (19b), yielding, in the "state-space" form,

$$\mathbf{Z}' = \tilde{\mathbf{A}}\mathbf{Z} + \mu\xi(\tau)\tilde{\mathbf{B}}\mathbf{Z}, \tag{20}$$

where $\mathbf{Z} = [X, Y, X', Y']$,

$$\tilde{\mathbf{A}} = \begin{bmatrix} 0 & 0 & 1 & 0 \\ 0 & 0 & 0 & 1 \\ -1 & \left(\frac{U_r^2}{2M_r}\frac{\partial C_D}{\partial Y} + \frac{U_r^2 KC_D}{M_r}\right) & -\left(2\zeta + \frac{U_r C_D}{M_r}\right) & \frac{U_r C_L}{2M_r} \\ 0 & -k^2\left(1 - \frac{U_r^2}{2M}\frac{\partial C_L}{\partial Y} - \frac{U_r^2 KC_L}{M_r}\right) & -\frac{kU_r C_L}{M_r} & -k\left(2\zeta + \frac{U_r C_D}{2M_r}\right) \end{bmatrix},$$

$$\tilde{\mathbf{B}} = \begin{bmatrix} 0 & 0 & 0 & 0 \\ 0 & 0 & 0 & 0 \\ 0 & 2\left(\frac{U_r^2}{2M_r}\frac{\partial C_D}{\partial Y} + \frac{U_r^2 KC_D}{M_r}\right) & -\frac{U_r C_D}{M_r} & \frac{U_r C_L}{2M_r} \\ 0 & 2\left(\frac{k^2 U_r^2}{2M_r}\frac{\partial C_L}{\partial Y} + \frac{k^2 U_r^2 KC_L}{M_r}\right) & -\frac{kU_r C_L}{M_r} & -\frac{kU_r C_D}{2M_r} \end{bmatrix}.$$

If there is no turbulence in the approach flow, the stability of Eq. (20) is determined by the eigenvalues of the system matrix $\tilde{\mathbf{A}}$. If the real part of an eigenvalue is positive, the system is unstable. When upstream turbulence is significant, the stability of Eq. (20) depends on $\tilde{\mathbf{A}}$, $\tilde{\mathbf{B}}$, and the characteristics of the noise term $\xi(t)$. Thus a stochastic method (Section 4) has to be utilized in order to explore the stability of the system.

4. Moment Lyapunov exponent

Consider a linear stochastic system governed by the following equations of motion:

$$\dot{\tilde{\mathbf{x}}} = \tilde{\mathbf{A}}\tilde{\mathbf{x}} + \varepsilon\xi(t)\tilde{\mathbf{B}}\tilde{\mathbf{x}}, \quad \tilde{\mathbf{x}} \in \mathbb{R}^4, \tag{21}$$

where ε is a small parameter. Assume that system (21) has one critical mode and one stable mode. Let $\mathbf{x}=\mathbf{T}\tilde{\mathbf{x}}$, where the matrix of transformation $\mathbf{T}$ is constructed from the eigenvectors of $\tilde{\mathbf{A}}$. Specifically, if the eigenvalues consist of two complex-conjugate pairs $\lambda_{1,2}=-\varepsilon^2\delta_1\pm\imath\omega_1$ and $\lambda_{3,4}=-\delta_2\pm\imath\omega_2$, and if the eigenvectors associated with the eigenvalues are $\mathbf{V}_{1R}+\imath\mathbf{V}_{1I}$ and $\mathbf{V}_{2R}+\imath\mathbf{V}_{2I}$, respectively, $\mathbf{T}$ can be chosen as $\mathbf{T}=[\mathbf{V}_{1R}\,\mathbf{V}_{1I}\,\mathbf{V}_{2R}\,\mathbf{V}_{2I}]$. The transformation then yields

$$\dot{\mathbf{x}}=\mathbf{A}\mathbf{x}+\varepsilon\xi(t)\mathbf{B}\mathbf{x},\quad \mathbf{x}\in\mathbb{R}^4,$$

where

$$\mathbf{A}=\begin{bmatrix}-\varepsilon^2\delta_1 & \omega_1 & 0 & 0\\ -\omega_1 & -\varepsilon^2\delta_1 & 0 & 0\\ 0 & 0 & -\delta_2 & \omega_2\\ 0 & 0 & -\omega_2 & -\delta_2\end{bmatrix},\quad \mathbf{B}=\begin{bmatrix}K_{11} & K_{12} & M_{11} & M_{12}\\ K_{21} & K_{22} & M_{21} & M_{22}\\ N_{11} & N_{12} & L_{11} & L_{12}\\ N_{21} & N_{22} & L_{21} & L_{22}\end{bmatrix},$$

$\varepsilon^2\delta_1$ and δ_2 represent the real parts of the eigenvalues corresponding to the critical mode and stable mode, respectively, ω_1 and ω_2 are modal frequencies, and the matrix $\mathbf{B}$ is determined by $\mathbf{B}=\mathbf{T}\tilde{\mathbf{B}}\mathbf{T}^{-1}$. Applying the transformation

$$x_1=\mathrm{e}^{\rho}\cos\phi_1\cos\theta,\quad x_3=\mathrm{e}^{\rho}\cos\phi_2\sin\theta,$$

$$x_2=-\mathrm{e}^{\rho}\sin\phi_1\cos\theta,\quad x_4=-\mathrm{e}^{\rho}\sin\phi_2\sin\theta,$$

one can obtain the following set of equations for the amplitude ρ, phase variables (ϕ_1,ϕ_2,θ) and noise process ξ:

$$\dot{\rho}=\sum_{j=0}^{2}\varepsilon^j q_j(\phi_1,\phi_2,\theta,\xi),\quad \dot{\theta}=\sum_{j=0}^{2}\varepsilon^j s_j(\phi_1,\phi_2,\theta,\xi),$$

$$\dot{\phi}_i=\sum_{j=0}^{2}\varepsilon^j h_{ij}(\phi_1,\phi_2,\theta,\xi),\quad \mathrm{d}\xi=-\alpha\xi\,\mathrm{d}t+\sigma\,\mathrm{d}W(t).$$

In the above expressions, the phase angles ϕ_1 and ϕ_2 are in $(0,2\pi)$, θ is in $(0,\pi/2)$, expressions for the coefficients q_j, s_j, and h_{ij} are given in Appendix A, and α and σ are defined as in the previous section.

Since the processes $(\phi_1,\phi_2,\theta,\xi)$ do not depend on ρ, the processes $(\phi_1,\phi_2,\theta,\xi)$ form a diffusive Markov process and the associated generator is given by

$$\mathfrak{L}(p)=\mathfrak{L}_0(p)+\varepsilon\mathfrak{L}_1(p)+\varepsilon^2\mathfrak{L}_2(p),$$

where

$$\mathfrak{L}_0=\frac{\sigma^2}{2}\frac{\partial^2}{\partial\xi^2}-\alpha\xi\frac{\partial}{\partial\xi}+\sum_{i=1}^{2}\omega_i\frac{\partial}{\partial\phi_i}+s_0(\phi_1,\phi_2,\theta,\xi)\frac{\partial}{\partial\theta},$$

$$\mathfrak{L}_1=s_1(\phi_1,\phi_2,\theta,\xi)\frac{\partial}{\partial\theta}+\sum_{i=1}^{2}h_{i1}(\phi_1,\phi_2,\theta,\xi)\frac{\partial}{\partial\phi_i},$$

$$\mathfrak{L}_2=s_2(\phi_1,\phi_2,\theta,\xi)\frac{\partial}{\partial\theta}+\sum_{i=1}^{2}h_{i2}(\phi_1,\phi_2,\theta,\xi)\frac{\partial}{\partial\phi_i}.$$

Arnold et al. [21,22] have shown that $\Lambda(p)$ is an isolated simple eigenvalue of $L(p)$ with nonnegative eigenfunction ψ, i.e.

$$L(p)\psi=\Lambda(p)\psi\quad\text{for all real } p,\tag{22}$$

where

$$L(p)=L_0(p)+\varepsilon L_1(p)+\varepsilon^2 L_2(p)$$

and

$$L_0(p) = \mathfrak{L}_0 + pq_0, \quad L_1(p) = \mathfrak{L}_1 + pq_1, \quad L_2(p) = \mathfrak{L}_2 + pq_2.$$

A method of regular perturbation is applied to obtain a weak noise expansion of the moment Lyapunov exponent. Consider an expansion of the moment Lyapunov exponent in powers of ε:

$$\Lambda(p) = \Lambda_0(p) + \varepsilon\Lambda_1(p) + \varepsilon^2\Lambda_2(p) + \mathcal{O}(\varepsilon^2).$$

Substituting the above expansions into Eq. (22), one obtains the following equations:

$$(L_0(p) - \Lambda_0(p))\psi_0 = 0, \tag{23}$$

$$(L_0(p) - \Lambda_0(p))\psi_1 = \Lambda_1(p)\psi_0 - L_1(p)\psi_0, \tag{24}$$

$$(L_0(p) - \Lambda_0(p))\psi_2 = \Lambda_2(p)\psi_0 + \Lambda_1(p)\psi_1 - L_2(p)\psi_0 - L_1(p)\psi_1, \tag{25}$$

$$\vdots$$

4.1. Zeroth-order perturbation

From the definition of $\Lambda(p)$, $\Lambda_0(p) \equiv 0$ for all possible p. Thus, Eq. (23) reduces to

$$(\mathfrak{L}_0 + pq_0)\psi_0 = 0.$$

Using the method of separation of variables, one can easily obtain

$$\psi_0(\phi_1, \phi_2, \theta, \xi) = \psi_0(\theta) = (\cos\theta)^p. \tag{26}$$

The solution to the associated adjoint equation of Eq. (23) is

$$\Psi_0^* = \frac{Z_0^*(\xi)\delta_0}{4\pi^2},$$

where δ_0 is the Dirac delta function at 0, and $Z_0^*(\xi)$ is the stationary probability density of the Ornstein–Uhlenbeck process $\xi(t)$. Details of the zeroth-order perturbation are given in Appendix B

4.2. First-order perturbation

Substituting the above expression for $\psi_0(\theta)$ into Eq. (24) results in

$$L_0\psi_1 = -s_1(\phi_1, \phi_2, \theta, \xi)\frac{\mathrm{d}\psi_0}{\mathrm{d}\theta} + [\Lambda_1(p) - pq_1(\phi_1, \phi_2, \theta, \xi)]\psi_0. \tag{27}$$

From the Fredholm Alternative, for Eq. (27) to have a nontrivial solution it is required that

$$\langle -s_1\psi_0' + [\Lambda_1(p) - pq_1]\psi_0, \Psi_0^*\rangle = 0,$$

i.e.

$$\Lambda_1(p) = \langle s_1\psi_0' + pq_1\psi_0, \Psi_0^*\rangle = \frac{1}{16\pi^2}\langle \xi g(\phi_1, \phi_2, \theta), Z_0^*(\xi)\delta_0\rangle = 0, \tag{28}$$

where $\langle(\cdot),(\cdot\cdot)\rangle$ is the inner product defined by

$$\langle(\cdot),(\cdot\cdot)\rangle = \int_0^{\pi/2}\int_{-\infty}^{+\infty}\int_0^{2\pi}\int_0^{2\pi}(\cdot)(\cdot\cdot)\,\mathrm{d}\phi_1\,\mathrm{d}\phi_2\mathrm{d}\xi\,\mathrm{d}\theta,$$

$$\begin{aligned} g(\phi_1, \phi_2, \theta) = p(\cos\theta)^p\{&K_{22}\sin^2\phi_1 + K_{11}\cos^2\phi_1 - \tfrac{1}{2}(K_{12} + K_{21})\sin 2\phi_1 \\ &+ \tfrac{1}{2}\tan\theta[M_{11}(\cos\phi^+ + \cos\phi^-) - M_{22}(\cos\phi^+ - \cos\phi^-) \\ &- M_{12}(\sin\phi^+ - \sin\phi^-) - M_{21}(\sin\phi^+ + \sin\phi^-)]\}, \end{aligned}$$

in which $\phi^\pm = \phi_1 \pm \phi_2$.

The equality in Eq. (28) results from the fact that q_1 and s_1 are periodic in ϕ_1 and ϕ_2 (see Appendix A), and ξ is a zero mean process. Hence, Eq. (27) reduces to

$$\mathfrak{L}_0\psi_1 = -\xi g(\phi_1, \phi_2, \theta). \tag{29}$$

Eq. (29) can be solved by applying Duhamel's Principle and making use of the solution of the Fokker–Planck equation (15). For more details, refer to Zhu et al. [28]. Thus, the solution to Eq. (29) is given by

$$\begin{aligned}\psi_1(\phi_1, \phi_2, \theta, \xi) = & -\frac{1}{2}p(\cos\theta)^p\left\{K_{11}\left(G(2\phi_1) - \frac{1}{\alpha}\right) - K_{22}\left(G(2\phi_1) + \frac{1}{\alpha}\right) - (K_{12} + K_{21})H(2\phi_1)\right.\\ & + \tan\theta[M_{11}(G(\phi^+) + G(\phi^-)) - M_{22}(G(\phi^+) - G(\phi^-))\\ & \left.-M_{12}(H(\phi^+) - H(\phi^-)) - M_{21}(H(\phi^+) + H(\phi^-))]\right\}\xi(t),\end{aligned}$$

where the functions $G(\cdot)$ and $H(\cdot)$ are defined in Appendix C.

4.3. Second-order perturbation

The equation for the second-order perturbation is

$$L_0\psi_2 = [\Lambda_2(p) - L_2]\psi_0 - L_1\psi_1. \tag{30}$$

From the Fredholm Alternative, for Eq. (30) to have a nontrivial solution it is required that

$$\langle[\Lambda_2(p) - L_2]\psi_0 - L_1\psi_1, \Psi_0^*\rangle = 0,$$

i.e.

$$\begin{aligned}\Lambda_2(p) &= \langle L_2\psi_0 + L_1\psi_1, \Psi_0^*\rangle\\ &= \left\langle\left(s_2\frac{\partial}{\partial\theta} + pq_2\right)\psi_0 + \left(s_1\frac{\partial}{\partial\theta} + h_{11}\frac{\partial}{\partial\phi_1} + h_{21}\frac{\partial}{\partial\phi_2} + pq_1\right)\psi_1, \Psi_0^*\right\rangle.\end{aligned}$$

After performing the integration, one obtains

$$\Lambda_2(p) = [-8\delta_1 + (\kappa_2F_0 + \kappa_3F_1 + \kappa_4F_2 + \kappa_5F_3 + \kappa_6F_4)]\frac{p}{8} + \left(\kappa_2F_0 + \frac{2\kappa_1}{\alpha}\right)\frac{p^2}{16}, \tag{31}$$

where

$$\kappa_1 = (K_{11} + K_{22})^2, \quad \kappa_2 = (K_{12} + K_{21})^2 + (K_{11} - K_{22})^2,$$

$$\kappa_3 = (N_{12} + N_{21})(M_{11} - M_{22}) - (N_{11} - N_{22})(M_{12} + M_{21}),$$

$$\kappa_4 = (N_{12} + N_{21})(M_{12} + M_{21}) + (N_{11} - N_{22})(M_{11} - M_{22}),$$

$$\kappa_5 = (N_{11} + N_{22})(M_{12} - M_{21}) + (N_{12} - N_{21})(M_{11} + M_{22}),$$

$$\kappa_6 = (N_{11} + N_{22})(M_{11} + M_{22}) - (N_{12} - N_{21})(M_{12} - M_{21})$$

and

$$F_0 = \frac{\sigma^2}{\alpha^2 + 4\omega_1^2},$$

$$F_1 = \frac{\sigma^2(\omega_1 + \omega_2)}{\alpha[(\delta_2 + \alpha)^2 + (\omega_1 + \omega_2)^2]}, \quad F_2 = \frac{\sigma^2(\delta_2 + \alpha)}{\alpha[(\delta_2 + \alpha)^2 + (\omega_1 + \omega_2)^2]},$$

$$F_3 = \frac{\sigma^2(\omega_1 - \omega_2)}{\alpha[(\delta_2 + \alpha)^2 + (\omega_1 - \omega_2)^2]}, \quad F_4 = \frac{\sigma^2(\delta_2 + \alpha)}{\alpha[(\delta_2 + \alpha)^2 + (\omega_1 - \omega_2)^2]}.$$

The maximal Lyapunov exponent can be calculated by Eq. (7) as

$$\lambda = \varepsilon^2[-\delta_1 + \tfrac{1}{8}(\kappa_2 F_0 + \kappa_3 F_1 + \kappa_4 F_2 + \kappa_5 F_3 + \kappa_6 F_4)]. \tag{32}$$

From the above expressions, κ_1 and κ_2 are always positive. κ_3, κ_4, κ_5, and κ_6 can take on a positive or a negative value depending on the values of the elements of matrix **B**. Similarly, the parameters F_0, F_1, F_2, and F_4 are always positive, while the parameter F_3 can take on a positive or a negative value depending on the difference between frequencies. From Eq. (32), one can see that the stabilization is possible if the total contribution of turbulence is negative. If only x-direction motion is considered, Eqs. (31) and (32) reduce to equations in κ_1, κ_2, and F_0 only. Since they are all positive, the one degree-of-freedom system cannot be stabilized, which agrees with the results of Xie [29]. Since all F_i $(i = 0, 1, \ldots, 4)$ include the term σ^2/α, which represents the noise intensity, increasing the noise intensity can assist either the stabilization or the destabilization effect of noise.

5. Study of stabilization

5.1. Deterministic system

Uniform flow: As presented in Section 3, the model will reduce to that of Zhu et al. [4] in the lock-in range when the flow is uniform and laminar

$$Y'' + \left[2\zeta + \frac{U_r C_D}{2M_r} - \frac{U_r^2 c_d^y}{M_r}\right] Y' + Y = \frac{U_r^2 C_L}{2M_r}.$$

In the lock-in range, it can be shown that the vibration of the cylinder can be attributed to main resonance arising from the lock-in forcing, to parametric instability due to time-variant fluid damping, and to constant-fluid-damping-induced instability. The critical parameters are the motion-dependent damping coefficient and the bandwidth of vortex shedding. At high reduced velocities ($U_r > 20$), the motion-dependent force coefficients approach zero and can be neglected [30]. Furthermore, the vortex shedding frequency is far removed from the natural frequency of the cylinder, which eliminates the forced vibration due to vortex shedding. Hence, the system is expected to be stable.

Shear flow: At high reduced velocities, motion-dependent forces are assumed to be negligible. The equations of motion are thus reduced to those of Yu et al. [5]

$$X'' + \left(2\zeta + \frac{U_r C_D}{M_r}\right) X' + X - \left(\frac{U_r^2}{2M_r}\frac{\partial C_D}{\partial Y} + \frac{U_r^2 K C_D}{M_r}\right) Y - \frac{U_r C_L}{2M_r} Y' = \frac{U_r^2}{2M_r} C_D, \tag{33a}$$

$$Y'' + k\left(2\zeta + \frac{U_r C_D}{2M_r}\right) Y' + k^2\left(1 - \frac{U_r^2}{2M_r}\frac{\partial C_L}{\partial Y} - \frac{U_r^2 K C_L}{M_r}\right) Y + \frac{k U_r C_L}{M_r} X' = \frac{k^2 U_r^2}{2M_r} C_L. \tag{33b}$$

The equations of motion (33a), (33b) have a similar form to those for wake galloping. As such, the derivative $\partial C_L/\partial X$ is a critical parameter that determines instability [31]. The lift coefficient C_L and its derivative $\partial C_L/\partial Y$ are also expected to play a significant role in the stability of a cylinder in a shear flow.

For a cylinder in a shear flow, the drag and lift coefficients, C_D and C_L, respectively, are functions of the Reynolds number and the dimensionless shear parameter K. Since $U = U_0 + Gy$ is a function of y only, the derivatives of C_D and C_L with respect to x are zero. The derivatives of C_D and C_L with respect to y can be evaluated as

$$\frac{\partial C_D}{\partial y} = \frac{\partial C_D}{\partial Re}\frac{\partial Re}{\partial y} + \frac{\partial C_D}{\partial \mathrm{K}}\frac{\partial K}{\partial y}, \tag{34a}$$

$$\frac{\partial C_L}{\partial y} = \frac{\partial C_L}{\partial Re}\frac{\partial Re}{\partial y} + \frac{\partial C_L}{\partial \mathrm{K}}\frac{\partial K}{\partial y}. \tag{34b}$$

After normalization, Eqs. (34a), (34b) can be written as

$$\frac{\partial C_D}{\partial Y} = \frac{\partial C_D}{\partial Re} Re\, K - \frac{\partial C_D}{\partial K} K^2, \tag{35a}$$

$$\frac{\partial C_L}{\partial Y} = \frac{\partial C_L}{\partial Re} Re\, K - \frac{\partial C_L}{\partial K} K^2. \tag{35b}$$

If extensive data of $C_D(Re, K)$ and $C_L(Re, K)$ are known, their derivatives with respect to Y can be calculated by Eqs. (35a), (35b).

In order to demonstrate the fluidelastic instability of the system described by Eqs. (33a), (33b), consider an example with the parameters $Re = 100$, $M_r = 5112$, and $\zeta = 0.007$. At this Reynolds number, data on the variation of the drag and lift coefficients with Re and K are available from Lei et al. [32], and one finds

$$C_D = 1.486, \quad \frac{\partial C_D}{\partial K} = -0.32, \quad \frac{\partial C_D}{\partial Re} = -0.0016,$$

$$C_L = -0.126, \quad \frac{\partial C_L}{\partial K} = -1.0, \quad \frac{\partial C_L}{\partial Re} = 0.0005.$$

The stability depends on the eigenvalues of the system matrix $\mathbf{A}$. If the real parts of the eigenvalues are negative, the system is stable. When the reduced velocity increases to a critical value, the largest real part of the eigenvalues become positive, i.e., the cylinder becomes unstable. Increasing the shear parameter also tends to destabilize the cylinder. For example, the critical velocity for $k = 1.0$ is $U_{r,\mathrm{cr}} = 256$ at $K = 0.1$ and decreases to about $U_{r,\mathrm{cr}} = 112$ at $K = 0.2$. The stability boundary for a cylinder with $M_r = 5112$ is determined experimentally by Yu et al. [5] as approximately $U_r K^{1.44}/2\pi = 5$, which yields $U_{r,\mathrm{cr}} = 865$ at $K = 0.1$. Clearly, the results presented here do not agree quantitatively with the stability boundary obtained by Yu et al. [5]. The discrepancies can be attributed to the fact that the Reynolds number was changed from 8 to 120 in the experiments of Yu et al. [5] while the present results are obtained at $Re = 100$. The lift and drag force coefficients depend on the Reynolds number in this range. On the other hand, the effects of U_r and K on the stability are qualitatively the same as the experimental observations. Both sets of results show that increasing U_r or K can destabilize the cylinder. Similarly both sets of results indicate that increasing M_r, or decreasing either U_r or K weakens the effect of C_L, and thus makes the system more stable.

Similar to the case of galloping, the fluidelastic instability of a cylinder in a shear flow turns out to be sensitive to the ratio of natural frequencies in the two coordinate directions. Small changes of frequency can significantly shift the critical velocity (see Fig. 2(a)). The minimum critical velocity occurs at about $k = 0.95$, and the critical velocity increases rapidly with larger detuning in the frequencies. Note that this phenomenon is also observed in the flutter of a two-dimensional linear airfoil by Poirel and Price [17].

5.2. Stochastic system

Uniform flow: The effect of free-stream turbulence in a uniform approach flow has been studied recently by So et al. [33]. It was shown that the effect of free-stream turbulence in the case of a single cylinder in a cross-flow is to increase the amplitude of cylinder vibration in the U_r range of 1.45–12.08. This is due to an increase in the vortex-induced force in the U_r range of 1.45–7.25, and an increase in the fluid damping force in the U_r range of 8.21–12.08. However, no unstable motion was observed. When U_r is increased to very large values, as occurred in the present study, it is expected that the cylinder will remain stable.

Shear flow: When grid-generated turbulence is added to the flow, the governing equations of the cylinder (Eqs. (19a), (19b)) are random differential equations. The Lyapunov exponent and moment Lyapunov exponent of the system can be determined using the analytical method developed in Section 4. The critical reduced velocity for the deterministic and stochastic systems are obtained and are shown in Fig. 2. From Fig. 2(a), one can see that turbulence can shift the critical reduced velocity to a higher value and thus stabilize the system. Fig. 2(b) gives the stabilized percentage $r_{U_{r,\mathrm{cr}}}$ of the critical reduced velocity and also shows that the stabilization effect becomes smaller when α increases from 0.3 to 0.6. For each value of α, μ varies with α from 1.0 to $\sqrt{2}$ in such a way that the turbulence intensity remains fixed, where the formula for turbulence intensity

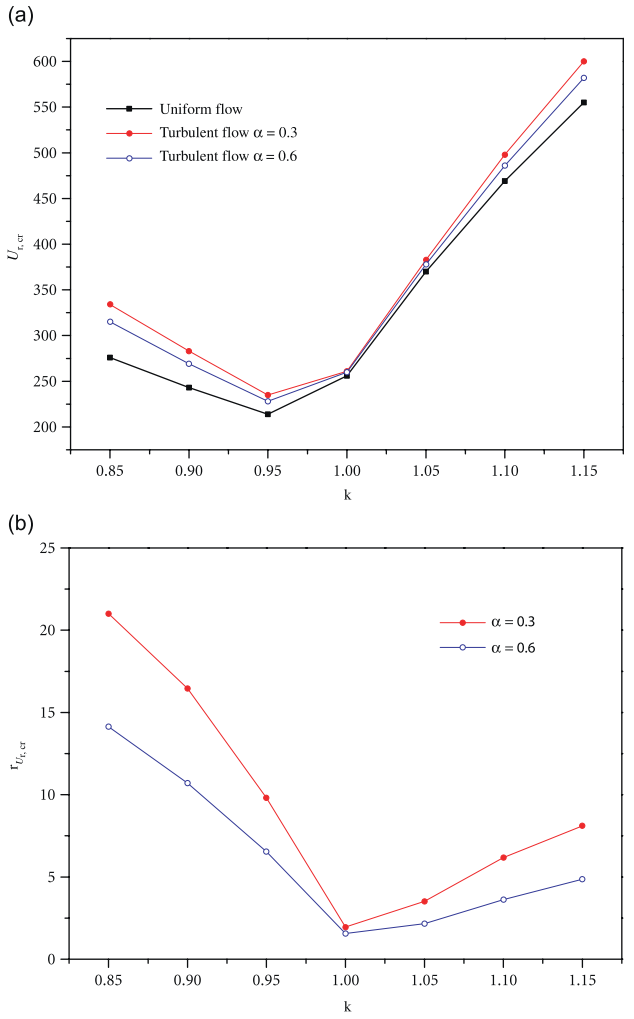

Fig. 2. Turbulence effects for different frequency ratio k with fixed T_u. (a) The critical reduced velocity U_r; (b) the stabilized percentage $r_{U_{r,cr}}$ of the critical reduced velocity.

is given by

$$T_u = \frac{\mu\sigma_\xi}{\sqrt{2\alpha}}. \tag{36}$$

Since α is related to the integral length L_x, this result implies that L_x is a key parameter for stabilization. The effect of μ on the stability is shown in Fig. 3. When μ increases, the critical reduced velocity at which the Lyapunov exponent is zero is shifted to a higher value. Since α is fixed and σ_ξ is chosen to be 0.5 for all cases, this means that higher turbulence intensity can achieve a better stabilization effect.

It is also found that the stabilization effect of turbulence is sensitive to the ratio of frequencies k, as shown in Fig. 2. Comparison of the critical velocities for different cases ($k = 0.85-1.15$) in Fig. 2 shows that the stabilization effect is more significant with larger detuning in frequencies. When there is no detuning ($k = 1$), turbulence increases the critical reduced velocity slightly from $U_{r,\mathrm{cr}} = 256$ to 261. When k increases or decreases from 1, the differences in the critical reduced velocity increase significantly. For example, for $k = 0.9$ and $\mu = 0.6$, the critical reduced velocity increases from $U_{r,\mathrm{cr}} = 243$ for uniform flow to $U_{r,\mathrm{cr}} = 283$ for turbulent flow with $\mu = 0.6$. To illustrate the influence of k, two cases ($k = 1$ and 0.9) are considered here.

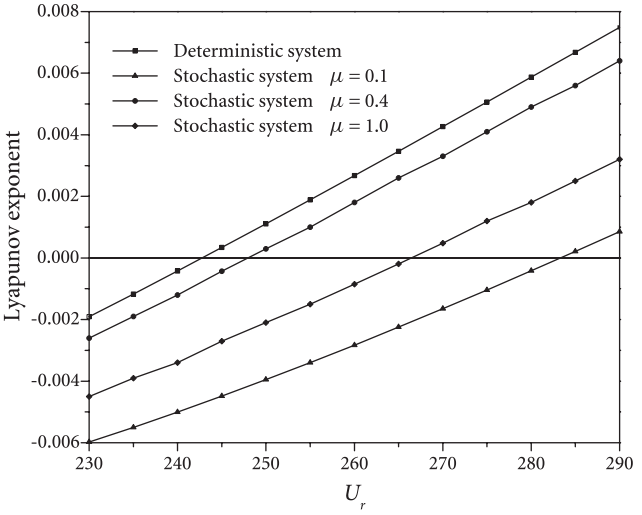

Fig. 3. Stability boundary for $k = 0.9$ and $\alpha = 0.3$.

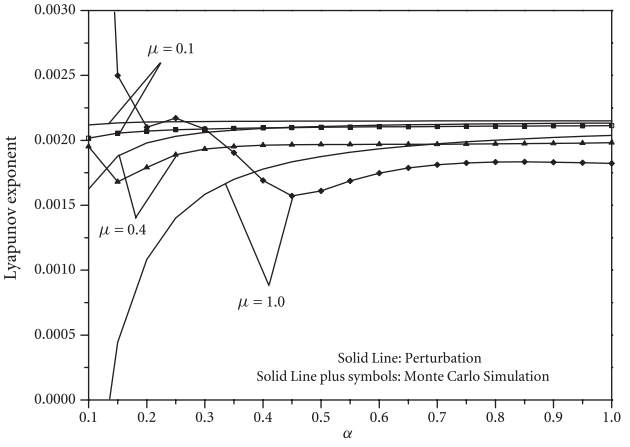

Fig. 4. Lyapunov exponent for $k = 1.0$ and $U_r = 280$.

For a cylinder in a shear flow with $k = 1.0$ and $U_r = 280$, the system matrices **A** and **B** are given by

$$\mathbf{A} = \begin{bmatrix} 0.00215 & 0.97696 & 0 & 0 \\ -0.97696 & 0.00215 & 0 & 0 \\ 0 & 0 & -0.07719 & 1.06005 \\ 0 & 0 & -1.06005 & -0.07719 \end{bmatrix},$$

$$\mathbf{B} = \begin{bmatrix} -0.00610 & -0.01270 & -0.05120 & 0.00657 \\ 0.04164 & 0.05830 & -0.01271 & 0.08690 \\ 0.04965 & 0.05741 & -0.16954 & 0.15978 \\ -0.01000 & -0.01749 & -0.04129 & -0.00474 \end{bmatrix}.$$

The Lyapunov exponents can be calculated from Eq. (32) for different values of α and μ as shown in Fig. 4. It can be seen that Lyapunov exponents are decreased slightly when α is decreased or μ is increased. However, this stabilization effect is quite small and is not enough to stabilize the system. This is due to the weak interaction between the two modes, which can be seen from matrix **B**. The elements M_{ij} and N_{ij} in the upper right submatrix and lower left submatrix are relatively small. Thus, the sum of the product of κ_{i+2} and F_i $(i = 0, 1, \ldots, 4)$ in Eq. (32) is small and the largest Lyapunov exponent remains positive.

When $k = 0.9$ and $U_r = 260$, the system matrices **A** and **B** are given by

$$\mathbf{A} = \begin{bmatrix} 0.00267 & 0.91588 & 0 & 0 \\ -0.91588 & 0.00267 & 0 & 0 \\ 0 & 0 & -0.07076 & 1.01278 \\ 0 & 0 & -1.01278 & -0.07076 \end{bmatrix},$$

$$\mathbf{B} = \begin{bmatrix} 0.07601 & 0.02414 & 0.06375 & -0.01045 \\ 0.01608 & 0.00607 & -0.02520 & -0.00767 \\ -0.31696 & -0.10233 & -0.19893 & 0.05301 \\ -0.05759 & -0.01817 & -0.05297 & 0.00725 \end{bmatrix}.$$

These two cases have similar matrix **A**. However, N_{11} and N_{12} in matrix **B** are relatively large compared to those for $k = 1$, which means that stronger interactions between two modes exist when the difference of frequencies increases. Thus, energy can be transmitted from the critical mode to the stable mode via turbulence, which results in stabilization. Rottmann and Popp [11] also reported the experimental observation that the rocking mode of vibration switched from stable to unstable at high turbulence intensities in a fully flexible bundle while the translational mode was stabilized. This partially proved the energy transfer between two coupling modes.

The Lyapunov exponents for $k = 0.9$ is shown in Fig. 5. The stabilization effect increases with a decrease of α or an increase of noise intensity μ. The same conclusion can also be drawn from moment Lyapunov exponents shown in Figs. 6 and 7. It can be seen that the slope at $p = 0$ for $\mu = 0.1$ is positive, which means that the system is unstable. When μ increases, the slope at $p = 0$ becomes negative and the system becomes stable. Furthermore, the moment Lyapunov exponents are negative between $p = 0$ and 0.8 for $\mu = 1$ as shown in Fig. 6, which demonstrates the moment stability of the system. From these figures, it is found that the system is stabilized in the sense of both sample stability and moment stability.

The Lyapunov exponents and moment Lyapunov exponents can also be obtained by Monte Carlo simulation (see, e.g., Ref. [23]). In the simulation, the system (Eqs. (19)) can be discretized using a Euler

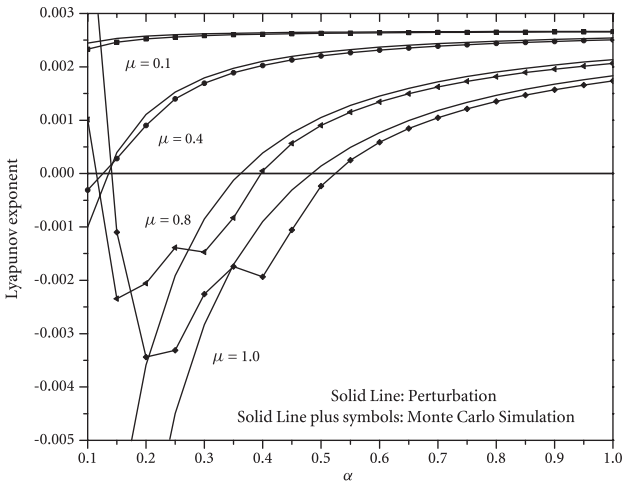

Fig. 5. Lyapunov exponent for $k = 0.9$ and $U_r = 260$.

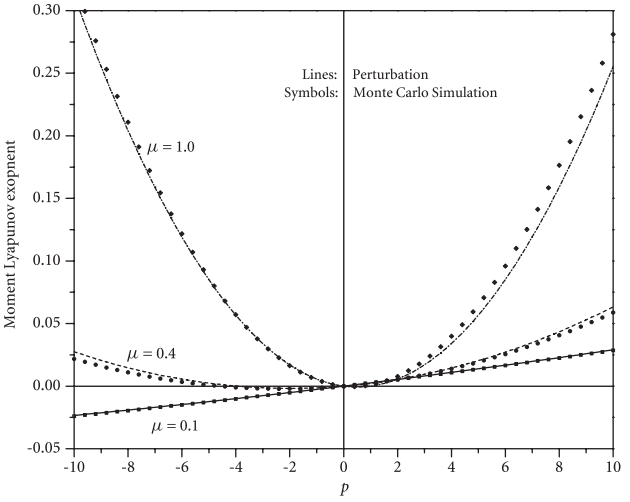

Fig. 6. Moment Lyapunov exponent for $\alpha = 0.3$, $k = 0.9$, and $U_r = 260$.

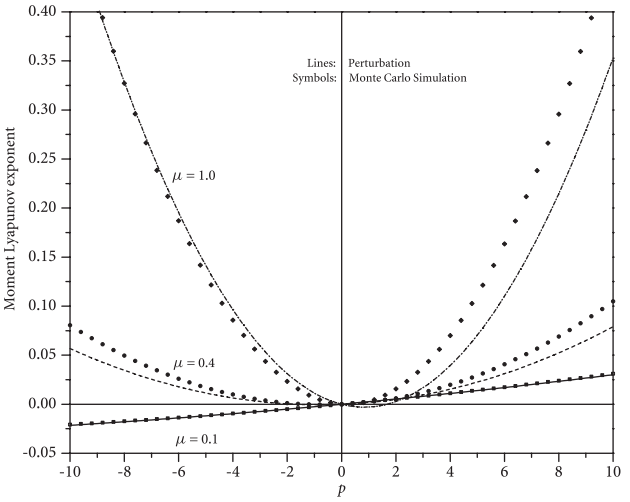

Fig. 7. Moment Lyapunov exponent for $\alpha = 0.2$, $k = 0.9$, and $U_r = 260$.

scheme with a time step $\Delta t = 10^{-6}$. Five thousand sample paths are simulated to calculate the moment Lyapunov exponents. As shown in Figs. 5–7, the numerical results agree well with the analytical results for larger values of α. One exception is Fig. 4 which shows significant discrepancies even when α is large. This is because all the elements of matrix $\mathbf{B}$ are small compared to the value of μ, which negatively impacts the accuracy of the perturbation method. For all cases shown in Fig. 4, the discrepancy increases with decreasing values of α. Figs. 6 and 7 also show that the perturbation results are better with relatively large values of α. The power spectrum of real noise is more narrow-banded for the smaller values of α. The discrepancy can be explained by the fact that one assumption for using perturbation method is that the noise is wide-banded. Numerical results show that turbulence can destabilize the system when $\alpha < 0.1$. One possible explanation is that the destabilization is due to parametric resonance. When α is small, the energy of the real noise is located in the lower frequency range. Since the difference between ω_1 and ω_2 is small, parametric resonance corresponding to a combination difference type could occur [17].

As mentioned in Section 4, the stabilization effect is more significant with decreasing α or increasing μ. Thus, the stabilization effect is proportional to the turbulence intensity, which agrees with the experimental observations of Rottmann and Popp [11]. Experiments by Romberg and Popp [10] show that stabilization can

be observed when turbulence intensity T_u is larger than 13%. In the present study, stabilization occurs at $T_u = 6.5\%$ ($\mu = 0.1$ and $\alpha = 0.3$) (see Fig. 3). However, the effect of turbulence on the fluid force coefficients is not taken into account in the present study. This is due to the lack of relevant experimental data for a cylinder in a shear flow. In reality, the coefficients can be influenced by the turbulence intensity and the Reynolds number [9,34]. Further experimental investigation on the effect of turbulence will be conducted in the future.

6. Conclusions

In this paper, the effect of real noise on the stability of a parametrically excited four-dimensional system is considered. The dynamic stability of the system is studied by determining the moment Lyapunov exponents and the Lyapunov exponents. For weak noise excitations, a regular perturbation method is employed to obtain second-order expansions of the moment Lyapunov exponents. The Lyapunov exponent is then obtained using the relationship between the moment Lyapunov exponent and the Lyapunov exponent. This analytical method is applied to a circular cylinder in a shear flow, which is subjected to fluidelastic instability.

The analysis demonstrates that the cylinder can be stabilized by the real noise in the sense of both sample stability and moment stability when proper parameters are selected. It is found that the stabilization is sensitive to the frequency ratio k. A larger detuning can result in a better stabilization effect due to stronger coupling between the two modes. Furthermore, the stabilization effect is proportional to the turbulence intensity, which agrees with the experimental observations. The accuracy of the approximate analytical results is determined by comparing them with numerical simulations.

Acknowledgment

Funding support from the Research Grant Council of the Government of the HKSAR under Project nos. PolyU5307/03E and PolyU5321/04E is gratefully acknowledged.

Appendix A. Transformation for polar coordinates

The transformation yields the following coefficients:

$$q_0(\phi_1,\phi_2,\theta,\xi) = -\delta_2 \sin^2\theta, \quad q_2(\phi_1,\phi_2,\theta,\xi) = -\delta_1 \cos^2\theta,$$

$$\begin{aligned} q_1(\phi_1,\phi_2,\theta,\xi) = [&\tfrac{1}{4}\sin 2\theta[(M_{11}+N_{11})(\cos\phi^+ + \cos\phi^-) - (M_{22}+N_{22})(\cos\phi^+ - \cos\phi^-) \\ &- (M_{21}+N_{12})(\sin\phi^+ + \sin\phi^-) - (M_{12}+N_{21})(\sin\phi^+ - \sin\phi^-)] \\ &+ \sin^2\theta[L_{11}\cos^2\phi_2 + L_{22}\sin^2\phi_2 - \tfrac{1}{2}(L_{12}+L_{21})\sin 2\phi_2)] \\ &+ \cos^2\theta[K_{11}\cos^2\phi_1 + K_{22}\sin^2\phi_1 - \tfrac{1}{2}(K_{12}+K_{21})\sin 2\phi_1]]\xi(t), \end{aligned}$$

$$h_{10}(\phi_1,\phi_2,\theta,\xi) = \omega_1, \quad h_{12}(\phi_1,\phi_2,\theta,\xi) = 0,$$

$$\begin{aligned} h_{11}(\phi_1,\phi_2,\theta,\xi) = [&K_{12}\sin^2\phi_1 - K_{21}\cos^2\phi_1 - \tfrac{1}{2}(K_{11}-K_{22})\sin 2\phi_1 \\ &- \tfrac{1}{2}\tan\theta[M_{21}(\cos\phi^+ + \cos\phi^-) + M_{12}(\cos\phi^+ - \cos\phi^-) \\ &+ M_{11}(\sin\phi^+ + \sin\phi^-) - M_{22}(\sin\phi^+ - \sin\phi^-)]]\xi(t), \end{aligned}$$

$$h_{20}(\phi_1,\phi_2,\theta,\xi) = \omega_2, \quad h_{22}(\phi_1,\phi_2,\theta,\xi) = 0,$$

$$\begin{aligned} h_{21}(\phi_1,\phi_2,\theta,\xi) = [&L_{12}\sin^2\phi_2 - L_{21}\cos^2\phi_2 - \tfrac{1}{2}(L_{11}-L_{22})\sin 2\phi_2 \\ &- \tfrac{1}{2}\cot\theta[N_{21}(\cos\phi^+ + \cos\phi^-) + N_{12}(\cos\phi^+ - \cos\phi^-) \\ &- N_{22}(\sin\phi^+ + \sin\phi^-) + N_{11}(\sin\phi^+ - \sin\phi^-)]]\xi(t), \end{aligned}$$

$$s_0(\phi_1,\phi_2,\theta,\xi) = -\tfrac{1}{2}\delta_2 \sin 2\theta, \quad s_2(\phi_1,\phi_2,\theta,\xi) = \tfrac{1}{2}\delta_1 \sin 2\theta,$$

$$\begin{aligned} s_1(\phi_1,\phi_2,\theta,\xi) = [&\tfrac{1}{4}\sin 2\theta[2L_{11}\cos^2\phi_2 + 2L_{22}\sin^2\phi_2 - (L_{12}+L_{21})\sin 2\phi_2 \\ &- 2K_{11}\cos^2\phi_1 - 2K_{22}\sin^2\phi_1 + (K_{12}+K_{21})\sin 2\phi_1] \\ &- \tfrac{1}{2}\sin^2\theta[M_{11}(\cos\phi^+ + \cos\phi^-) - M_{22}(\cos\phi^+ - \cos\phi^-) \\ &- M_{12}(\sin\phi^+ - \sin\phi^-) - M_{21}(\sin\phi^+ + \sin\phi^-)] \\ &+ \tfrac{1}{2}\cos^2\theta[N_{11}(\cos\phi^+ + \cos\phi^-) - N_{22}(\cos\phi^+ - \cos\phi^-) \\ &- N_{12}(\sin\phi^+ + \sin\phi^-) - N_{21}(\sin\phi^+ - \sin\phi^-)]]\xi(t). \end{aligned}$$

Appendix B. Zeroth-order perturbation

For zeroth-order perturbation, one has a deterministic system

$$\dot\rho = -\delta_2 \sin^2\theta, \quad \dot\theta = -\tfrac{1}{2}\delta_2 \sin 2\theta, \quad \dot\phi_i = \omega_i. \tag{B.1}$$

Solving Eq. (B.1), one obtains

$$\rho = -\delta_2 \int_0^t \sin^2\theta(s)\,\mathrm{d}s + \rho_0, \quad \theta = \tan^{-1}(\theta_0 \mathrm{e}^{-\delta_2 t}), \tag{B.2}$$

where ρ_0 and θ_0 are two constants which can be determined by the initial conditions. Since the zero-order system is deterministic, it follows from the definition of $\Lambda(p)$,

$$\Lambda_0(p) = \lim_{t\to\infty}\frac{1}{t} p \log\|x(t;x_0)\| = p\lambda_0, \tag{B.3}$$

where $\|x\| = \mathrm{e}^{\rho}$ and

$$\begin{aligned} \lambda_0 = \lim_{t\to\infty}\frac{\rho(t)}{t} &= -\delta_2 \lim_{t\to\infty}\frac{1}{t}\int_0^t \sin^2\theta(s)\,\mathrm{d}s \\ &= -\delta_2 \lim_{t\to\infty}\frac{1}{t}\int_0^t \frac{\tan^2\theta(s)}{1+\tan^2\theta(s)}\,\mathrm{d}s \\ &= -\delta_2 \lim_{t\to\infty}\frac{1}{t}\int_0^t \frac{\theta_0^2\mathrm{e}^{-2\delta_2 s}}{1+\theta_0^2\mathrm{e}^{-2\delta_2 s}}\,\mathrm{d}s = 0. \end{aligned}$$

Thus, $\Lambda_0(p) \equiv 0$ for all possible p. Eq. (23) reduces to

$$(\mathfrak{L}_0 + pq_0)\psi_0 = 0,$$

where

$$\mathfrak{L}_0 = \frac{\sigma^2}{2}\frac{\partial^2}{\partial\xi^2} - \alpha\xi\frac{\partial}{\partial\xi} + \omega_1\frac{\partial}{\partial\phi_1} + \omega_2\frac{\partial}{\partial\phi_2} - \frac{1}{2}\delta_2\sin 2\theta\frac{\partial}{\partial\theta}.$$

Applying the method of separation of variables and letting $\psi_0 = F(\theta)Z_0(\xi)H_1(\phi_1)H_2(\phi_2)$ results in

$$\frac{H_1'}{H_1} = a_1, \tag{B.4a}$$

$$\frac{H_2'}{H_2} = a_2, \tag{B.4b}$$

$$\frac{\sigma^2}{2}\frac{\ddot Z_0}{Z_0} - \alpha\zeta\frac{\dot Z_0}{Z_0} - \frac{1}{2}\delta_2\sin 2\theta\frac{F_\theta}{F} - p\delta_2\sin^2\theta = -(a_1+a_2). \tag{B.4c}$$

Solving equation for $H_1(\phi_1)$ yields $H_1(\phi_1) = Ae^{a_1\phi_1}$. For $H_1(\phi_1)$ to be a periodic function, it is required that $a_1 = 0$ and hence $H_1(\phi_1)$ can be chosen as 1. Similarly, $a_2 = 0$ and $H_2(\phi_2) = 1$. Hence, Eq. (B.4c) reduces to

$$\frac{\sigma^2}{2}\frac{\ddot{Z}_0}{Z_0} - \alpha\zeta\frac{\dot{Z}_0}{Z_0} = a, \tag{B.5a}$$

$$\frac{1}{2}\delta_2 \sin 2\theta \frac{F_\theta}{F} + p\delta_2 \sin^2\theta = a. \tag{B.5b}$$

Eq. (B.5a) is an eigenvalue problem with the eigenvalues given by $a = 0, -\alpha, -2\alpha, \ldots$ (see, e.g., Ref. [35]). However, the left-hand-side of Eq. (B.5b) goes to 0 since θ approaches 0 when $t \to \infty$. Thus, the constant a in Eqs. (45a), (45b) should be be taken as 0. The equation for $Z_0(\xi)$ becomes

$$\tfrac{1}{2}\sigma^2\ddot{Z}_0 - \alpha\xi\dot{Z}_0 = 0, \tag{B.6}$$

which can be easily solved to yield

$$Z_0(\xi) = C_1 \int \exp\left(\frac{\alpha}{\sigma^2}\xi^2\right)\mathrm{d}\xi + C_2, \quad -\infty < \xi < \infty.$$

For $Z_0(\xi)$ to be bounded, it is required that $C_1 = 0$ and hence $Z_0(\xi)$ can be taken as 1.

The equation for $F(\theta)$ becomes

$$\frac{\mathrm{d}F}{\mathrm{d}\theta} = (-p\tan\theta)F.$$

The solution to this equation is $F(\theta) = (\cos\theta)^p$. Therefore

$$\Lambda_0(p) = 0, \quad \psi_0(\phi_1, \phi_2, \theta, \xi) = \psi_0(\theta) = (\cos\theta)^p. \tag{B.7}$$

Since $\Lambda_0(p) = 0$, the associated adjoint differential equation of Eq. (23) is

$$L_0^*\Psi_0^* = \frac{\sigma^2}{2}\frac{\partial^2\Psi_0^*}{\partial\xi^2} + \alpha\xi\frac{\partial\Psi_0^*}{\partial\xi} + \alpha\Psi_0^* - \omega_1\frac{\partial\Psi_0^*}{\partial\phi_1} - \omega_2\frac{\partial\Psi_0^*}{\partial\phi_2} + \frac{1}{2}\delta_2\sin 2\theta\frac{\partial\Psi_0^*}{\partial\theta} + (\delta_2\cos 2\theta - p\delta_2\sin^2\theta)\Psi_0^* = 0. \tag{B.8}$$

Applying the method of separation of variables and letting $\Psi_0^*(\phi_1, \phi_2, \theta, \xi) = F^*(\theta)Z_0^*(\xi)H_1^*(\phi_1)H_2^*(\phi_2)$ leads to

$$\frac{(H_1^*)_{\phi_1}}{H_1^*} = b_1, \tag{B.9a}$$

$$\frac{(H_2^*)_{\phi_2}}{H_2^*} = b_2, \tag{B.9b}$$

$$\frac{\sigma^2}{2}\frac{\ddot{Z}_0^*}{Z_0^*} + \alpha\zeta\frac{\dot{Z}_0^*}{Z_0^*} + \alpha + \frac{1}{2}\delta_2\sin 2\theta\frac{(F^*)_\theta}{F^*} + (\delta_2\cos 2\theta - p\delta_2\sin^2\theta) = -(b_1 + b_2). \tag{B.9c}$$

The equation for H_1^* yields $H_1^*(\phi_1) = Be^{-b_1\phi_1}$. For $H_1^*(\phi_1)$ to be a periodic function, $b_1 = 0$ and $H_1^*(\phi_1)$ can be taken as

$$H_1^*(\phi_1) = \frac{1}{2\pi}, \quad 0 \leqslant \phi_1 < 2\pi.$$

Similarly, one has

$$H_2^*(\phi_2) = \frac{1}{2\pi}, \quad 0 \leqslant \phi_2 < 2\pi.$$

The above equations show that ϕ_1 and ϕ_2 are uniformly distributed between 0 and 2π. Hence, Eq. (B.9c) is reduced to

$$\frac{\sigma^2}{2}\frac{\ddot{Z}_0^*}{Z_0^*}+\alpha\zeta\frac{\dot{Z}_0^*}{Z_0^*}+\alpha=b, \tag{B.10a}$$

$$-\frac{1}{2}\delta_2\sin 2\theta\frac{(F^*)_\theta}{F^*}-(\delta_2\cos 2\theta-p\delta_2\sin^2\theta)=b. \tag{B.10b}$$

Based on the same reasoning as mentioned above, b should be taken as 0.

The equation for Z_0^* becomes

$$\tfrac{1}{2}\sigma^2\ddot{Z}_0^*+\alpha\xi\dot{Z}_0^*+\alpha Z_0^*=0, \tag{B.11}$$

which is the Fokker–Planck equation for the stationary transition probability density of the Ornstein–Uhlenbeck process $\xi(t)$ as defined in Eq. (B.11). Eq. (B.11) may be written as

$$\frac{\mathrm{d}}{\mathrm{d}\xi}\left(\frac{\mathrm{d}Z_0^*}{\mathrm{d}\xi}+\frac{2\alpha}{\sigma^2}\zeta Z_0^*\right)=0$$

or

$$\frac{\mathrm{d}Z_0^*}{\mathrm{d}\xi}+\frac{2\alpha}{\sigma^2}\xi Z_0^*=C_3=\text{probability current}. \tag{B.11$'$}$$

Since the stationary probability density $Z_0^*(\xi)$ and the probability current vanishes when $\xi\to\pm\infty$, the constant of integration $C_3=0$. Eq. (B.11′) can be easily solved to give

$$Z_0^*(\xi)=C_4\exp\left(-\frac{\alpha}{\sigma^2}\xi^2\right).$$

Since $Z_0^*(\xi)$ is the stationary probability density, normalizing it yields

$$Z_0^*(\xi)=\frac{1}{\sqrt{2\pi}\sigma_z}\exp\left(-\frac{\xi^2}{2\sigma_z^2}\right), \tag{B.12}$$

i.e. the Ornstein–Uhlenbeck process $\xi(t)$ is a normally distributed random variable with mean $\mu_\xi=0$ and standard deviation $\sigma_z=\sigma_\xi/\sqrt{2\alpha}$.

The equation for $F^*(\theta)$ becomes

$$\frac{1}{2}\sin 2\theta\frac{\mathrm{d}F^*}{\mathrm{d}\theta}=(\cos 2\theta-p\sin^2\theta)F^*. \tag{B.13}$$

Since $\theta=0$ is a stable equilibrium point of system (B.1), by following Pardoux and Wihstutz [36] the solution can be chosen as

$$F^*(\theta)=\delta_0,$$

where δ_0 is the Dirac delta function at 0.

Hence, the solution to Eq. (B.8) is obtained as

$$\Psi_0^*=\frac{Z_0^*(\xi)\delta_0}{4\pi^2}.$$

Appendix C. Expressions in first-order perturbation

The following functions are used to express the solution to Eq. (28):

$$G(2\phi_1)=\frac{2\omega_1\sin 2\phi_1-\alpha\cos 2\phi_1}{\alpha^2+4\omega_1^2},$$

$$H(2\phi_1) = -\frac{2\omega_1 \cos 2\phi_1 + \alpha \sin 2\phi_1}{\alpha^2 + 4\omega_1^2},$$

$$G(\phi^{\pm}) = \frac{[(\omega_1 \pm \omega_2)\sin(\phi^{\pm}) - (\delta_2 + \alpha)\cos(\phi^{\pm})]}{(\delta_2 + \alpha)^2 + (\omega_1 \pm \omega_2)^2},$$

$$H(\phi^{\pm}) = -\frac{[(\omega_1 \pm \omega_2)\cos(\phi^{\pm}) + (\delta_2 + \alpha)\sin(\phi^{\pm})]}{(\delta_2 + \alpha)^2 + (\omega_1 \pm \omega_2)^2}.$$

References

[1] E. Naudascher, D. Rockwell, *Flow-induced Vibrations: An Engineering Guide*, Balkema Publishers, USA, 1994.
[2] T. Sarpkaya, Vortex-induced oscillations—a selective review, *ASME Journal of Applied Mechanics* 46 (1979) 241–258.
[3] T. Sarpkaya, A critical review of the intrinsic nature of vortex-induced oscillations, *Journal of Fluids and Structures* 19 (2004) 389–447.
[4] J. Zhu, X.Q. Wang, W.-C. Xie, R.M.C. So, Flow-induced instability under bounded noise excitation in cross-flow, *Journal of Sound and Vibration* 312 (2008) 476–495.
[5] M. Yu, C. Yu, K. Chen, Fluid elastic instability of a small circular cylinder in the shear layer of a two-dimensional jet, *Physics of Fluids* 16 (7) (2004) 2357–2370.
[6] A. Bokaian, F. Geoola, Wake-induced galloping of two interfering circular cylinders, *Journal of Fluid Mechanics* 146 (1984) 383–415.
[7] S.J. Price, M.P. Paidoussis, An improved mathematical model for stability of cylinder rows subject to cross-flow, *Journal of Sound and Vibration* 97 (4) (1984) 615–640.
[8] S.S. Chen, *Flow-Induced Vibration of Circular Cylindrical Structures*, Hemisphere Publishing, New York, 1987.
[9] R.M.C. So, S.D. Savkar, Buffeting forces on rigid circular cylinders in cross flows, *Journal of Fluid Mechanics* 105 (1981) 397–425.
[10] O. Romberg, K. Popp, The influence of upstream turbulence of the stability boundaries of a flexible tube in a bundle, *Journal of Fluids and Structures* 12 (1998) 153–169.
[11] M. Rottmann, K. Popp, Influence of upstream turbulence on the fluidelastic instability of a parallel triangular tube bundle, *Journal of Fluids and Structures* 18 (2003) 595–612.
[12] C.G. Bucher, Y.K. Lin, Stochastic stability of bridges considering coupled modes, *Journal of Engineering Mechanics* 114 (12) (1988) 2055–2071.
[13] L. Arnold, Stabilization of linear-systems by noise, *SIAM Journal on Control and Optimization* 21 (3) (1983) 451–461.
[14] L. Arnold, Stabilization by noise revisited, *Zeitschrift Fur Angewandte Mathematik Und Mechanik* 70 (7) (1990) 235–246.
[15] M.D. Pandey, S.T. Ariaratnam, Stability analysis of wind-induced torsional motion of slender bridges, *Structural Safety* 20 (1998) 379–389.
[16] G. Rzentkowski, J.H. Lever, An effect of turbulence on fluidelastic instability in tube bundles: a nonlinear analysis, *Journal of Fluids and Structures* 12 (1998) 561–590.
[17] D. Poirel, S.J. Price, Random binary (coalescence) flutter of a two-dimensional linear airfoil, *Journal of Fluids and Structures* 18 (2003) 23–42.
[18] N. Sri Namachchivaya, L. Vedula, Stabilization of linear systems by noise: application to flow induced oscillations, *Dynamics and Stability of Systems* 15 (2) (2000) 185–208.
[19] R.A. Ibrahim, Excitation-induced stability and phase transition: a review, *Journal of Vibration and Control* 12 (10) (2006) 1093–1170.
[20] L. Arnold, A formula connecting sample and moment stability of linear stochastic systems, *SIAM Journal of Applied Mathematics* 44 (1984) 793–802.
[21] L. Arnold, E. Oeljeklaus, E. Pardoux, Almost sure and moment stability for linear itô equations, in: L. Arnold, V. Wihstutz (Eds.), *Lyapunov Exponents, Lecture Notes in Mathematics*, Vol. 1186, Springer, Berlin, 1986, pp. 85–125.
[22] L. Arnold, W. Kliemann, E. Oeljeklaus, Lyapunov exponents of linear stochastic systems, in: L. Arnold, V. Wihstutz (Eds.), *Lyapunov Exponents, Lecture Notes in Mathematics*, Vol. 1186, Springer, Berlin, 1986, pp. 129–159.
[23] W.-C. Xie, *Dynamic Stability of Structures*, Cambridge University Press, New York, 2006.
[24] X.Q. Wang, R.M.C. So, K.T. Chan, A nonlinear fluid force model for vortex-induced vibration of an elastic cylinder, *Journal of Sound and Vibration* 260 (2003) 287–305.
[25] G.K. Batchelor, *The Theory of Homogeneous Turbulence*, Cambridge University Press, Cambridge, 1953.
[26] S.B. Pope, *Turbulent Flows*, Cambridge University Press, New York, 2000.
[27] S. Kang, Uniform-shear flow over a circular cylinder at low Reynolds numbers, *Journal of Fluids and Structures* 22 (2006) 541–555.
[28] J. Zhu, W.-C. Xie, R.M.C. So, Stabilization of a four-dimensional system under real noise excitation, in: C. Constanda, S. Potapenko (Eds.), *Integral Methods in Science and Engineering: Theoretical and Practical Aspects*, Birkhauser, Boston, 2007.
[29] W.-C. Xie, Moment Lyapunov exponents of a two-dimensional system in wind-induced vibration under real noise excitation, *Chaos, Solitons and Fractals* 14 (2002) 349–367.

[30] S.S. Chen, Y. Cai, G.S. Srikantiah, Fluid damping controlled instability of tubes in crossflow, *Journal of Sound and Vibration* 217 (1998) 883–907.
[31] R.D. Blevins, *Flow-Induced Vibration*, second ed., Van Nostrand Reinhold, New York, 1990.
[32] C. Lei, L. Cheng, K. Kavanagh, A finite difference solution of the shear flow over a circular cylinder, *Ocean Engineering* 27 (2000) 271–288.
[33] R.M.C. So, X.Q. Wang, W.-C. Xie, J. Zhu, Free-stream turbulence effects on vortex-induced vibration of an elastic cylinder, *Journal of Fluids and Structures* 24 (2008) 481–495.
[34] H.M. Blackburn, W.H. Melbourne, The effect of free-stream turbulence on sectional lift forces on a circular cylinder, *Journal of Fluid Mechanics* 11 (1996) 267–292.
[35] C.W. Gardiner, *Handbook of Stochastic Methods for Physics, Chemistry and the Natural Sciences*, Springer, New York, 1985.
[36] E. Pardoux, V. Wihstutz, Lyapunov exponent and rotation number of two-dimensional linear stochastic systems with small diffusion, *SIAM Journal on Applied Mathematics* 48 (2) (1988) 442–457.